bioRxiv preprint doi: https://doi.org/10.1101/2022.05.20.491674; this version posted May 23, 2022. The copyright holder for this preprint (which was not certified by peer review) is the author/funder. All rights reserved. No reuse allowed without permission.

An iPSC library from a family with Creutzfeldt-Jakob disease caused by the E200K mutation

Nhat T.T. Le[1#], Robert C.C. Mercer[1#], Aldana D. Gojanovich[2#], Seonmi Park[2], Bei Wu[1], Gustavo Mostoslavsky[2, 3, 4*] & David A. Harris[1*]

[1]Department of Biochemistry, Boston University School of Medicine, Boston, Massachusetts, 02118, United States of America
[2]Center for Regenerative Medicine of Boston University and Boston Medical Center, Boston, Massachusetts, 02118, United States of America
[3]Department of Microbiology, Boston University School of Medicine, Boston, Massachusetts, 02118, United States of America
[4]Department of Medicine, Boston University School of Medicine, Boston, Massachusetts, 02118, United States of America

[#]equal contributions

*To whom correspondence should be addressed: gmostosl@bu.edu & daharris@bu.edu

Summary

Familial Creutzfeldt-Jakob disease (fCJD) caused by the E200K mutation of the prion protein (PrP) is the most common subtype of genetic prion disease. We have generated a library of human induced pluripotent stem cells (iPSCs) derived from a family with the E200K mutation, comprised of 11 carriers and 11 non-carriers. A comparison of neurons derived from E200K iPSCs to those from non-carriers revealed the presence of several disease-relevant phenotypes. Although traditional proteinase K resistant, detergent-insoluble, and seed-competent PrP was not observed, neurons derived from E200K carriers were found to contain thioflavin S positive PrP puncta. At the postsynaptic site, the co-localization of N-Methyl-D-aspartic acid receptors and post synaptic density 95 colocalization was disrupted in neurons expressing E200K PrP. Our study shows that iPSC-derived neurons, which express endogenous levels of mutant PrP in a human neuronal context, can model certain aspects of human prion disease, offering a powerful platform for investigating pathological mechanisms and testing potential therapeutics.

bioRxiv preprint doi: https://doi.org/10.1101/2022.05.20.491674; this version posted May 23, 2022. The copyright holder for this preprint (which was not certified by peer review) is the author/funder. All rights reserved. No reuse allowed without permission.

Introduction

Prion diseases are a group of invariably fatal neurodegenerative conditions affecting a wide range of mammalian species. This group includes animal diseases such as bovine spongiform encephalopathy, scrapie, which afflicts sheep and goats, and chronic wasting disease (CWD) which affects free-ranging cervid populations in North America, Asia and Europe. In humans, prion diseases include Creutzfeldt-Jakob disease (CJD), Gerstmann-Sträussler-Scheinker disease (GSS), fatal familial insomnia (FFI) and kuru (Cohen & Prusiner, 1998; Mercer *et al.*, 2018a; Prusiner, 1998). The key molecular event underlying these disorders is a structural transformation of the cellular prion protein (PrP^{C}), a normal cell-surface glycoprotein, into a pathogenic, amyloid conformation, denoted PrP^{Sc} (Kamali-Jamil *et al.*, 2021; Kraus *et al.*, 2021; Vázquez-Fernández *et al.*, 2016). This structural rearrangement endows PrP^{Sc} with the ability to catalyze its own formation through a self-templating mechanism, and imparts upon it distinct biochemical attributes, including resistance to protease digestion and insolubility in detergents (Meisl *et al.*, 2021; Mercer, *et al.*, 2018a). In humans, the etiology of these diseases is threefold; i) sporadic CJD is by far the most common human prion disease and accounts for ~85% of all cases, ii) a small proportion is due to infection through iatrogenic means or through consumption of contaminated tissues, and iii) ~15% of cases are inherited in an autosomal dominant manner due to point and insertion/deletion mutations in *PRNP,* the gene encoding the prion protein (Kim *et al.*, 2018; Wadsworth & Collinge, 2007).

In humans, the most prevalent prion disease associated mutation is a substitution of glutamic acid for lysine at residue 200 (E200K) which causes CJD. This is a highly

bioRxiv preprint doi: https://doi.org/10.1101/2022.05.20.491674; this version posted May 23, 2022. The copyright holder for this preprint (which was not certified by peer review) is the author/funder. All rights reserved. No reuse allowed without permission.

pathogenic mutation, displaying almost 100% penetrance (Minikel *et al.*, 2016; Chapman *et al.*, 1994). CJD-E200K patients most commonly present with dementia, ataxia and myoclonus; a combination of other symptoms such as pyramidal signs, Parkinsonism and dystonia are less frequently present. Spongiform change, neuronal loss, and gliosis predominate in the neocortex, basal ganglia, thalamus, and substantia nigra. Diffuse synaptic immunostaining of PrP is present in virtually all CJD-E200K patients. However a more plaque-like deposition predominates in individuals who are heterozygous (methionine/valine) at the polymorphic residue 129 (Kovacs *et al.*, 2011). The identity of this residue is known to have profound effects upon the presentation and/or disease course of many human prion diseases, however neither the clinical presentation nor pattern of spongiosis associated with CJD-E200K appear to be influenced by this polymorphism (Goldfarb *et al.*, 1992; Kovacs *et al.*, 2011; Palmer *et al.*, 1991). Pathological tau deposition can also be found in more than 90% of CJD-E200K patients (Kovacs *et al.*, 2011).

In experimental settings, it is possible to transmit prions to immortalized cell lines, brain slices, and laboratory rodents. Several experimental systems have been used previously to model inherited prion diseases, including those caused by the E200K mutation. Work from our laboratory demonstrated that, when overexpressed in CHO cells, E199K PrP (the mouse homologue of the E200K human mutation) acquired some of the biochemical properties of prions, including detergent insolubility and resistance to protease digestion (Lehmann & Harris, 1996a, 1996b). However, immortalized cells (perhaps with one exception (Schätzl *et al.*, 1997)) do not exhibit signs of toxicity upon

bioRxiv preprint doi: https://doi.org/10.1101/2022.05.20.491674; this version posted May 23, 2022. The copyright holder for this preprint (which was not certified by peer review) is the author/funder. All rights reserved. No reuse allowed without permission.

prion infection, making them unsuitable to examine the mechanisms underlying prion-induced cytopathology (Mercer & Harris, 2019). Extensive research has focused on the development of E200K transgenic mice, but none of the existing models fully recapitulate all features of the disease. Mice expressing the mutated human protein do not develop disease (Asante *et al.*, 2009), and while mice expressing the mutation in the context of a mouse/human hybrid PrP do succumb to a neurodegenerative syndrome, pathological changes such as vaccuolation and prion deposition are minor and protease resistant PrP is not typical of that found in CJD-E200K (Friedman-Levi *et al.*, 2011, 2013).

While much information can be learned from the study of post-mortem human brain tissue (Kovacs *et al.*, 2011), the ability to study the properties and toxicity of mutant PrP expressed at endogenous levels by human neurons has, until recently, not been possible. Human pluripotent stem cells (hPSCs), including embryonic stem cells (ESCs) (Thomson *et al.*, 1998) and induced pluripotent stem cells (iPSC) (Takahashi *et al.*, 2007), have enabled unprecedented opportunities to study the development of the human brain and the pathobiology of human disorders (Yamanaka, 2012). Recently, human iPSCs expressing wild-type PrP have been used to generate cerebral organoids (COs), which were shown to be capable of propagating sporadic CJD prions (Groveman *et al.*, 2019). However, COs generated from an iPSC line expressing E200K PrP did not contain any detectable PrP^{Sc}, and displayed no PrP or tau-related pathology (Foliaki *et al.*, 2020; Gonzalez *et al.*, 2018). Hyperphosphorylated tau has been noted in iPSC-derived neurons expressing PrP with a substitution of tyrosine for asparagine at residue 218 (Y218N), which is associated with GSS, demonstrating that at least some aspects of

bioRxiv preprint doi: https://doi.org/10.1101/2022.05.20.491674; this version posted May 23, 2022. The copyright holder for this preprint (which was not certified by peer review) is the author/funder. All rights reserved. No reuse allowed without permission.

inherited prion disease can be modeled using iPSC derived systems (Matamoros-Angles *et al.*, 2018).

Here, we describe a library of iPSCs obtained from an Israeli family harboring the E200K PrP mutation. To our knowledge, this is the first report of iPSC lines derived from multiple members of a single family carrying a prion-related mutation. We have performed a preliminary analysis of cortical pyramidal neurons derived from these iPSCs, and find that neurons from E200K carriers display specific biochemical and synaptic abnormalities not seen in neurons from non-carriers. This new resource represents a powerful experimental platform for dissection of the molecular mechanisms underlying human prion diseases.

bioRxiv preprint doi: https://doi.org/10.1101/2022.05.20.491674; this version posted May 23, 2022. The copyright holder for this preprint (which was not certified by peer review) is the author/funder. All rights reserved. No reuse allowed without permission.

Results

Generation of an iPSC library and differentiation into cortical neurons

We consented 22 individuals, including 11 carriers of the E200K PrP mutation, as well as 11 non-carriers. (Table 1). Peripheral blood mononuclear cells (PBMC) were collected and expanded *in vitro* using established procedures (C. A. Sommer *et al.*, 2012). These cells were then reprogrammed to generate iPSC lines in the absence of serum or a xenogeneic feeder layer (Figure 1A) (Park & Mostoslavsky, 2018). Expression of TRA-1-81, a marker of pluripotency, was assessed by immunofluorescence staining (Figure 1B).

Next, we differentiated 12 of these iPSC lines, including two control lines derived from unrelated individuals (BU1 and BU3; Table 1), into cortical pyramidal neurons through dual SMAD inhibition (Shi *et al.*, 2012). We adopted this differentiation protocol since it is widely used and relatively simple to perform; resulting in a relatively low percentage of astrocytes (<10%) and because the cerebral cortex is a prominent site of neuropathology in E200K patients (Kovacs *et al.*, 2011). iPSCs were differentiated in a stepwise manner (Figure 2A) going first through a neural stem cell stage (Figure Ci) before entering a progenitor phase within cellular aggregates known as rosettes which are positive for primary progenitor markers Pax6 and Nestin (Figure 2Cii, vi). Further neuronal induction leads to secondary progenitors, as evidenced by positive staining for TBR2 (Figure 2Cix). In the final stage of differentiation, these cells progress into mature neurons which are capable of generating Na^+/K^+-dependent action potentials (Figure 2B). The presence of fully differentiated neurons is further evidenced by the appearance of

bioRxiv preprint doi: https://doi.org/10.1101/2022.05.20.491674; this version posted May 23, 2022. The copyright holder for this preprint (which was not certified by peer review) is the author/funder. All rights reserved. No reuse allowed without permission.

typical pyramidal morphology including long neuronal processes (Figure 2Civ), dendritic spine formation (Figure 2Cv) and increased expression of neuronal markers Tuj1, Map2, Vglut1 and Satb2 (Figure 2Cvii, viii, x, xi).

E200K PrP from human iPSC derived neurons has some PrP^{Sc}-like properties

PrP^{C} is widely expressed in the CNS and is particularly abundant in neurons, where its expression level increases during development and neuronal differentiation (Adle-Biassette *et al.*, 2006; Steele *et al.*, 2006; Taraboulos *et al.*, 1992; Tremblay *et al.*, 2007). We first examined the expression level of PrP^{C} by western blotting. These analysis revealed a similar level of PrP^{C} expression across all lines of iPSC-derived neurons at 95 days post differentiation (Figure 3A).

Protease-resistant PrP^{Sc} is readily detected in the post-mortem brains of CJD-E200K patients (Kovacs *et al.*, 2011), symptomatic transgenic mice expressing the equivalent mutation in the context of a mouse/human chimeric PrP (Friedman-Levi *et al.*, 2011) and to a lesser extent in CHO cells overexpressing the equivalent mutation of mouse PrP (E199K) (Lehmann & Harris, 1996a, 1996b). Accordingly, we performed a number of biochemical assays to detect pathologically folded PrP in our collection of iPSC derived neurons expressing E200K PrP. First, we examined the proteinase K (PK) resistance of PrP in neuronal lysates by western blotting. Consistent with previous studies using fibroblasts derived from patient skin biopsy or cerebral organoids, we were unable to detect PK resistant PrP in neuronal lysates at 95 days post differentiation using 2.5 µg/ml of enzyme (Figure 3B) (Foliaki *et al.*, 2020; Rosenmann *et al.*, 2001). Next, we

bioRxiv preprint doi: https://doi.org/10.1101/2022.05.20.491674; this version posted May 23, 2022. The copyright holder for this preprint (which was not certified by peer review) is the author/funder. All rights reserved. No reuse allowed without permission.

assessed the detergent solubility of PrP as this characteristic is known to be observable before the emergence of protease resistance (Daude *et al.*, 1997). However, following centrifugation at 120 000 x g for 1 hour in the presence of 0.5% Triton X-100 and sodium deoxycholate, we were unable to detect any PrP in the insoluble fraction (Figure 3C).

We reasoned that pathological PrP may be present in these cells, but at levels too low to be appreciable by western blotting. To investigate this possibility, we adopted an immunocytochemical assay to visualize abnormally folded PrP. The amyloidogenic dye thioflavin S (ThS) was used to visualize β-sheet-rich protein deposits and immunostaining to detect PrP, thus revealing pathologically folded PrP as ThS and antibody positive puncta. As a positive control, we used mouse neuroblastoma cells (N2a) that are chronically infected with Rocky Mountain Lab (RML; a mouse-adapted sheep prion strain) prions (ScN2a) (Figure 4A). Areas of co-localization between PrP and ThS were detected, which were absent in uninfected N2a cells (Figure 4A, -PK, white arrowheads). This co-localization became more pronounced upon exposure to PK to digest residual PrP^{C} (Figure 4A, +PK, white arrowhead). We found that neurons from E200K carriers contained small but detectable numbers of PrP+/ThS+ puncta after PK treatment that were not present in neurons from non-carriers or control individuals ($p=0.0017$ (BU + NC vs. E200K) and $p=0.02$ (NC vs. E200K)) (Figure 4C, D).

To determine the seed competence of the observed ThS+ PrP, we turned to Real-Time Quaking-Induced Conversion (RT-QuIC) (Orrú *et al.*, 2015). This assay monitors PrP aggregation by measuring thioflavin T fluorescence, which increases in the presence

bioRxiv preprint doi: https://doi.org/10.1101/2022.05.20.491674; this version posted May 23, 2022. The copyright holder for this preprint (which was not certified by peer review) is the author/funder. All rights reserved. No reuse allowed without permission.

of amyloid structures. Bank vole PrP was chosen as the recombinant substrate, as it is a "universal acceptor" of prions from many species and has been shown to be able to detect CJD-E200K prions (Orrú *et al.*, 2015). RT-QuIC is extremely sensitive to the presence of prion seeds; in our hands, we can robustly detect seeding activity in RML infected brain homogenate up to a dilution of 10^{-7} (Figure 5A) and from lysates of ScN2a cells using as little as 2 pg of total protein (Figure 5B). When used to assay 2 ng of iPSC derived neuronal cell lysate, we were unable to reliably detect seeding activity (Figure 5C). One of five duplicate wells containing CJD29 lysate returned positive during the assay, which could indicate the presence of some seed competent PrP in this lysate near the limit of detection of the RT-QuIC assay. Interestingly, this is the line that displayed the greatest number of ThS+/PrP+ puncta (Figure 4B, D).

E200K neurons show a trend toward abnormal tau accumulation

Abnormally phosphorylated, intraneuronal deposits of tau are frequently observed by immunohistochemical staining in the brains of patients harbouring the E200K mutation, and these sometimes co-localize with misfolded forms of PrP (Kovacs *et al.*, 2011). In some cases, these phosphorylated tau species can also be observed by western blotting. We investigated whether these features could be observed in iPSC-derived neurons from E200K carriers. The levels of phospho-tau (T231) in relation to total tau by western blot was not significantly different between E200K and NC neurons (Figure S1A, B). Immunofluorescence staining revealed that E200K neurons displayed a trend toward increased numbers of p-tauT231-positive puncta compared to NC neurons, although this difference did not reach statistical significance ($p = 0.07$) (Figure S1C, D).

bioRxiv preprint doi: https://doi.org/10.1101/2022.05.20.491674; this version posted May 23, 2022. The copyright holder for this preprint (which was not certified by peer review) is the author/funder. All rights reserved. No reuse allowed without permission.

E200K neurons show synaptic abnormalities

We next turned our attention to characterizing the synapses spontaneously formed by these iPSC derived neuronal cultures. N-Methyl-D-aspartic acid receptors (NMDARs), the primary mediators of excitatory postsynaptic signaling, are stabilized at the synaptic site by the scaffolding protein post synaptic density 95 (PSD95) (Kornau *et al.*, 1995). Of particular relevance to the current study is the finding that PrP^C may physically interact with some NMDAR subunits (Khosravani *et al.*, 2008). Using immunofluorescence, we assessed the synaptic localization of NMDARs by staining for the obligatory NMDAR1 subunit and PSD95 (Figure 6A, B). Because the synaptic localization of NMDARs increases with development (Li *et al.*, 2003), we performed these experiments with neurons at 95 days post differentiation, at which point they had matured and displayed an electrically excitable, neuronal phenotype (Figure 2B). To score colocalization, we graphed the pixel intensity from each fluorescent channel along the length of the dendrite, defining co-localization as areas of significant overlap (Figure 6C; dashed boxes). We observed significantly reduced co-localization of NMDAR1 and PSD95 staining in E200K neurons compared to neurons derived from non-carriers (Figure 6D; BU + NC vs. E200K. $p=0.007$; NC vs. E200K, $p=0.04$). This observation is not due to a change in density of either protein separately, as there was no significant difference between E200K and control neurons in the density of NMDAR1 or PSD95 dendritic clusters (Figure 6E, F).

bioRxiv preprint doi: https://doi.org/10.1101/2022.05.20.491674; this version posted May 23, 2022. The copyright holder for this preprint (which was not certified by peer review) is the author/funder. All rights reserved. No reuse allowed without permission.

Discussion

The CJD-causing E200K mutation is the most common PrP mutation linked to familial prion disease. In this study, we created a bank of iPSCs from a large Israeli family, which we differentiated into neurons with the characteristics of cortical projection neurons using dual SMAD signaling inhibition. In a preliminary characterization of these neurons, we detected abnormal accumulations of PrP by immunofluorescence, as well as a disturbed alignment of NMDARs and PSD95 in the postsynaptic membrane. Together, our results lay the foundation for understanding the pathogenic mechanisms underlying the E200K mutation in a cell culture system based on human neurons from patients with defined, and ongoing, clinical histories.

In previous studies, we found that PrP molecules carrying several disease-linked mutations, including E200K, exhibited biochemical properties characteristic of PrP^{Sc}, including detergent-insolubility and mild protease-resistance, when expressed in transfected, immortalized cell lines in culture. In the current study, we did not detect detergent-insoluble or protease-resistant PrP in differentiated E200K neurons using these methods. However, we did observe small numbers of PrP-containing, ThS-positive deposits by immunofluorescence in the E200K neurons that were not present in neurons derived from non-carriers. This result suggests that the mutant PrP begins a misfolding process, but does not accumulate to levels detectable by biochemical techniques during the 95 days of culture used in our study. The biochemical discrepancies between data obtained using transfected lines of immortalized cells and iPSC-derived neurons may be a reflection of the differences in expression level; iPSC-derived neurons have

bioRxiv preprint doi: https://doi.org/10.1101/2022.05.20.491674; this version posted May 23, 2022. The copyright holder for this preprint (which was not certified by peer review) is the author/funder. All rights reserved. No reuse allowed without permission.

physiological expression levels of PrP while the transfected cell lines from previous work expressed much higher levels. Consistent with this explanation, cerebral organoids derived from E200K iPSCs also failed to accumulate detergent insoluble and protease resistant PrP. In contrast, insoluble, protease-resistant PrP was detected in the brains of Tg(E199K) mice, but in this case the mutant protein was also over-expressed compared to the WT protein. The low or undetectable levels of PrP^{Sc} present in our E200K neurons and in cerebral organoids correlates with the lack of seeding detected in these systems when assayed by RT-QuIC.

Accumulations of abnormally phosphorylated tau have been detected by both western blotting and immunofluorescence in the postmortem brains of CJD patients carrying the E200K mutation. While iPSC-derived E200K neurons showed a trend toward the accumulation of phospho-tau, this did not reach statistical significance; perhaps because we did not analyze a sufficient number of non-carrier neurons. Another possibility is that the tau misfolding/hyperphosphorylation process proceeds slowly when driven by physiological expression levels of mutant PrP and a longer period in culture is required for these deposits to become detectable. Increased levels of phosphorylated tau were observed in iPSC derived neurons expressing Y218N PrP after ~40 days in culture, suggesting that different mutations may have different pathological effects on neurons.

Glutamate receptor-dependent excitotoxicity is observed in many neurodegenerative diseases including Alzheimer's (Hynd *et al.*, 2004), amyotrophic lateral sclerosis (King *et al.*, 2016), Parkinson's (Ambrosi *et al.*, 2014) and Huntington's

bioRxiv preprint doi: https://doi.org/10.1101/2022.05.20.491674; this version posted May 23, 2022. The copyright holder for this preprint (which was not certified by peer review) is the author/funder. All rights reserved. No reuse allowed without permission.

(Sepers & Raymond, 2014). Because of this, as well as our observation that exogenously applied prions cause selective, NMDAR-dependent postsynaptic degeneration in primary cultures of hippocampal neurons (Fang *et al.*, 2018), we decided to investigate the integrity of the postsynaptic site. Interestingly, we observed a small, but statistically significant decrease in co-localization of NMDAR1 and PSD95 staining in E200K neurons, suggesting a disturbance of the postsynaptic architecture. PSD95 is a scaffolding protein that physically interacts with the cytoplasmic tails of the NR2 subunits of the NMDAR, and serves to anchor the receptors to the postsynaptic site. The lack of co-localization of PSD95 and NMDAR1 may reflect early stages of synapse disassembly. It remains to be determined whether there are electrophysiological correlates of this synaptic misalignment. Of note, PrP has been shown to interact physically with the NR2D subunit of NMDARs, raising the possibility that alterations in this function resulting from the E200K mutation could cause changes in the localization of the obligatorily associated NR1 subunit. Further experiments will be needed to delve further into the effects of E200K on synaptic structure and function.

In summary, we have generated a bank of iPSC lines from a family with an inherited prion disease due to the E200K PrP mutation. In the future, we plan to use this collection to explore key questions in the pathogenesis of inherited prion disease, including correlations of age of onset to biochemical and cellular abnormalities, the effects of the mutation on the function of iPSC-derived glial cells, the role of genetic modifiers of disease, and the efficacy of potential pharmacological interventions.

bioRxiv preprint doi: https://doi.org/10.1101/2022.05.20.491674; this version posted May 23, 2022. The copyright holder for this preprint (which was not certified by peer review) is the author/funder. All rights reserved. No reuse allowed without permission.

Materials and Methods

Generation of iPSC library

We collected peripheral blood from family members in Israel. Reprogramming was performed on frozen mononuclear cells shipped to Boston. Derivation of iPSCs was performed as described (Park & Mostoslavsky, 2018; Somers *et al.*, 2010; Sommer *et al.*, 2009). Briefly, 4 mL of peripheral blood was collected from all individuals, and the frozen isolated peripheral mononuclear cells were thawed, expanded in vitro and reprogrammed using Sendai virus vector (CytoTune-iPS 2.0 Sendai Reprogramming Kit from Invitrogen) using a feeder-free system (A. G. Sommer *et al.*, 2012; Staerk *et al.*, 2010). At least three independent clones were established, expanded, and saved from each individual. iPSCs were then characterized by immunofluorescence staining. The culture medium was aspirated, and cells were washed twice with 1X Dulbecco's Phosphate Buffered Saline (DPBS, Life Technologies, 14040-133). The cells were then fixed in 4% paraformaldehyde/DPBS (PFA, Electron Microscopy Sciences, 15710) for 20 min at room temperature (RT), then rinsed three times with PBS-T (0.2 % Tween-20/DPBS) for 5 min (Boston Bioproducts, 1BB-181), followed by a 10 min of permeabilization with 0.1% Triton X-100/DPBS at RT. Next, the cells were washed and incubated with 4 % normal goat serum/DPBS at RT for 2 h. The iPSC were then incubated with TRA-1-81 primary antibody (EMD Millipore, MAB4381) overnight at 2–8 °C, washed, and the secondary antibody, Alexa Fluor 488 conjugated goat anti-mouse immunoglobulin M was added (Thermo Fisher, A21042). All human subject studies were performed under signed consent and approved by the Boston University Institutional Review Board protocol H-32506.

bioRxiv preprint doi: https://doi.org/10.1101/2022.05.20.491674; this version posted May 23, 2022. The copyright holder for this preprint (which was not certified by peer review) is the author/funder. All rights reserved. No reuse allowed without permission.

Neuronal cell culture differentiated from hiPSCs

Neuronal differentiation was carried out described (Shi *et al.*, 2012). Briefly, iPSC lines were cultured in mTeSR™ 1 medium (STEMCELL Technologies) on a matrigel (BD Matrigel™, hESC-qualified Matrix, 354277) coated dish. When the confluence of iPSCs in two wells of a 6-well plate reached 95%, the cells were detached with ReLeSR™ (STEMCELL Technologies) and replated onto one matrigel-coated well. When the cells reached full confluence after 1–2 days, the medium was changed to neural induction media composed of neural maintenance media (1:1 mixture of DMEM/F-12 GlutaMAX: Neurobasal media supplemented with 0.5x N-2 (Life Technologies 17502048), 0.5x B-27 (Life Technologies 17504044), 2.5 µg/ml insulin (Sigma I9278), 1mM L-glutamine (Life Technologies 31331), 0.5x nonessential amino acids (Life Technologies 11140), 50 µM 2-mercaptoethanol (Life Technologies 31350), 0.5mM sodium pyruvate (Sigma S8636), 50 U/ml penicillin and 50 mg/ml streptomycin (Life Technologies 15140)) supplemented with 10 µM SB431542 (Tocris) and 1 µM Dorsomorphin (Tocris), so as to induce neuronal differentiation. This day is considered day 1. By day 12 following induction with daily media changes, the cells have formed a dense neuro-epithelial sheet. Cells were passaged with dispase (STEMCELL Technologies) to two laminin (1-ug/ml) coated wells. Following cell reattachment, the medium is changed to neural maintenance medium. FGF2 is added the following day to a concentration of 20 ng/ml. After 4 days of treatment with FGF2, it is withdrawn. Cells can be split 1:2 with dispase when rosettes start to meet, or if neural crest cells begin to appear. Careful dispase passaging leaves undifferentiated cells attached, but allows neural rosettes to lift off the substrate. On day 25 after induction (±1 day), cells are dissociated to single cells with Accutase™ (STEMCELL Technologies)

bioRxiv preprint doi: https://doi.org/10.1101/2022.05.20.491674; this version posted May 23, 2022. The copyright holder for this preprint (which was not certified by peer review) is the author/funder. All rights reserved. No reuse allowed without permission.

at a ratio of 1:1 into new laminin coated wells. As neurons are fragile, survival rate after passage is low. For this reason, cells were passaged for the final time around day 35 on poly-L-ornithine/ laminin coated vessels. Media is changed daily and mature neuronal samples are collected at day 95 of differentiation for further analysis.

Electrophysiology

Recordings were made from iPSC-derived neurons 60 -110 days after induction. Whole-cell patch clamp recordings were collected using standard techniques. Pipettes were pulled from borosilicate glass and polished to an open resistance of 2–5 megaohms. Experiments were conducted at room temperature with the following solutions: internal, 140 mM Cs-gluconate, 5 mM CsCl, 4 mM MgATP, 1 mM Na_2GTP, 10 mM EGTA, and 10 mM HEPES (pH 7.4 with CsOH); external, 150 mM NaCl, 4 mM KCl, 2 mM $CaCl_2$, 2 mM $MgCl_2$, 10 mM glucose, and 10 mM HEPES (pH 7.4 with NaOH). Signals were collected from a Multiclamp 700B amplifier (Molecular Devices, Sunnyvale, CA), digitized with a Digidata 1550A interface (Axon Instruments, Union City, CA), and saved to disc for analysis with PClamp 10 software.

Immunocytochemical analysis

iPSCs-derived neurons were grown on poly-L-ornithine/ laminin coated coverslips for microscopy. After washing in PBS, cells were fixed using 4% (w/v) PFA (Sigma) in PBS for 15 min and permeabilized with 0.1% Triton X-100 (Sigma) in PBS for 5 min, washed and blocked in 1% BSA (Sigma) in PBS for 30 minutes. Cells were stained using the primary and secondary antibodies listed (Table S1). Neurons were mounted in

bioRxiv preprint doi: https://doi.org/10.1101/2022.05.20.491674; this version posted May 23, 2022. The copyright holder for this preprint (which was not certified by peer review) is the author/funder. All rights reserved. No reuse allowed without permission.

Vectashield Mounting Medium and images were acquired using a Zeiss LSM 700 or 880 Laser Scanning Confocal Microscope with Airyscan with a 63x objective. Quantification experiments were carried out on 30-50 neurons for each line.

Western blotting

Cells were lysed with RIPA buffer (50 mM Tris base, 150 mM NaCl, 0.1% SDS, 0.5% sodium deoxycholate, 0.5% NP40) containing protease inhibitors (ThermoFisher) and a BCA assay was performed to determine protein concentration (Pierce). After boiling in sample buffer samples were electrophoresed with 12% Criterion TGX precast gels (BioRad) and transferred to PVDF membranes (Millipore). Membranes were blocked with 5% milk in TBS with 0.1% tween 20 (Fisher). Membranes were incubated overnight in the indicated primary antibody and after washing were incubated in the appropriate HRP-conjugated secondary antibody for two hours at room temperature (BioRad), washed again, exposed to ECL (Millipore) and visualized with a Gel Doc (BioRad). Quantification was performed using ImageJ. p values were determined using the student's t-test.

Detergent insolubility assay

One-tenth volume of 10x detergent was added to cell lysate to a final concentration of 0.5% Triton X-100 and 0.5% sodium deoxycholate. Samples were incubated for 10 min on ice, and debris removed by spinning at 1000 g for 5 min at 4 ℃. Samples were then centrifuged at 120000 x g for 40 min at 4 ℃ using a TLA-55 rotor. Supernatant (S) and pellet (P) samples were then analyzed by western blotting.

bioRxiv preprint doi: https://doi.org/10.1101/2022.05.20.491674; this version posted May 23, 2022. The copyright holder for this preprint (which was not certified by peer review) is the author/funder. All rights reserved. No reuse allowed without permission.

Detection of pathological forms of prion protein by immunofluorescence and Thioflavin S staining

PrP^{Sc} was revealed by exposure to PK and treatment with guanidine hydrochloride to remove PrP^{C} and expose PrP^{Sc} as described (Goold *et al.*, 2011; Veith *et al.*, 2009). N2a and ScN2a cells were seeded to semi-confluence on glass coverslips (pretreated with poly-L-lysine (0.2mg/ml) for 1h at RT) for 24h. iPSC derived neurons were cultured on poly-L-ornithine/ laminin coated coverslips. Cells were washed with PBS, and simultaneously fixed with freshly prepared paraformaldehyde (4% for non-PK treatment, 8% for PK treatment) and permeabilized with 0.1% Triton-X 100 for 1h at RT. Cells were then exposed to PK (5 µg/ml) for 10 min at 37 °C (stopped with 2mM PMSF (Sigma) for 15 min), as indicated. Cells were then incubated with 6M guanidine hydrochloride for 10 minutes. After blocking with 1% BSA for 30 min at RT, the cells were incubated with 0.025% of thioflavin S for 8 min and washed three times with 80% ethanol for 5 min. PrP was detected using antibody D18 in 1% BSA in PBS overnight at 4 °C followed by goat anti human-Alexa fluor 594 in 1% BSA in PBS for 45 min. Finally, cells were washed with PBS, counterstained with DAPI to reveal nuclei, and mounted in Vectashield Mounting Medium. The fluorescence was measured in at least 10 randomly chosen observation fields for each experimental condition using Zeiss LSM 880 Laser Scanning Confocal Microscope with Airyscan. Total Cell Fluorescence (CTCF) was calculated using the formula: CTCF = Integrated density – (Area of selected cell X Mean fluorescence of Background readings) using the ImageJ 2.0.0 Software (NIH). Quantification experiments were carried out independently at least three times; more than 30 neurons were counted for each condition.

bioRxiv preprint doi: https://doi.org/10.1101/2022.05.20.491674; this version posted May 23, 2022. The copyright holder for this preprint (which was not certified by peer review) is the author/funder. All rights reserved. No reuse allowed without permission.

Real Time-Quaking Induced Conversion (RT-QuIC) Assay

Recombinant bank vole PrP (residues 23 to 230; Methionine at position 109; accession no. AF367624) was expressed and purified as described previously (Orrú *et al.*, 2015). The concentration of recPrP was determined using a molar extinction coefficient at 280 nm of 62,005/M/cm. The protein was aliquoted and stored at -80 °C until use. RT-QuIC reactions were performed in black clear bottom 96-well plates using a reaction mixture composed of 10 mM phosphate buffer (pH 7.4), 300mM NaCl, 0.001% SDS, 1 mM EDTA, 10 µM ThT and 0.1 mg/ml recombinant bank vole PrP (residues 23-230, methionine at residue 109, accession number AF367624.1) in a final volume of 98 µL and seeded with 2 µL of sample. Plates were sealed and incubated in a BMG Polarstar plate reader at 42 °C with cycles of 1 min of shaking (700 rpm double orbital) and 1 min of rest. ThT fluorescence measurements were taken every 15 min (450 ± 10 nm excitation and 480 ± 10 nm emission; bottom read; 20 flashes per well; manual gain of 2000; 20 s integration time). Data were analyzed using GraphPad Prism 8.

Statistical Analysis

We statistically analyzed variables of interest by study groups (NC vs. E200K) in mixed linear models that accounted for within-line clustering resulting from the analysis of multiple observations per cell line and assume a Gaussian distribution for these dependent variables. We employed a working correlation structure of compound symmetry to address this clustering which, if left unaccounted, would have produced estimates of standard error that would have been too small, leading to the possibility of unjustifiably declaring statistical significance for differences in mean values between the

bioRxiv preprint doi: https://doi.org/10.1101/2022.05.20.491674; this version posted May 23, 2022. The copyright holder for this preprint (which was not certified by peer review) is the author/funder. All rights reserved. No reuse allowed without permission.

study groups. We present the estimated means and standard errors from these mixed linear models. We define statistical significance where analyses have p values less than < 0.05.

bioRxiv preprint doi: https://doi.org/10.1101/2022.05.20.491674; this version posted May 23, 2022. The copyright holder for this preprint (which was not certified by peer review) is the author/funder. All rights reserved. No reuse allowed without permission.

Acknowledgements

The authors would like to acknowledge the contribution of the family, without which this work would not be possible. We would also like to acknowledge Professor Howard Cabral for assistance with statistical analysis. Nhat T.T. Le was supported by a Warren Alpert Distinguished Scholar Award (Ltr dtd 3/28/2019), and Robert C.C. Mercer by a grant from the Department of Defense (PR201695). Work in the Mostoslavsky lab is supported by NIH Grants N0175N92020C00005 and 1R01DA051889-01. Work in the Harris lab is supported by NIH R01 NS065244. This work was also supported by NIH grant 1R21NS111499-01 to GM and DAH.

Author Contributions

Conceptualization, Project administration, Funding acquisition and Supervision: GM & DAH; Resources: AA, GM & DAH; Data curation, Formal analysis: NTTL, RCCM, ADG, BW; Visualization: NTTL, RCCM, ADG; Investigation, Methodology: NTTL, RCCM, ADG, SP, BW; Writing – original draft: RCCM, DAH; Writing – review & editing: NTTL, RCCM, ADG, GM & DAH.

Declaration of Interests

The authors declare no competing interests.

bioRxiv preprint doi: https://doi.org/10.1101/2022.05.20.491674; this version posted May 23, 2022. The copyright holder for this preprint (which was not certified by peer review) is the author/funder. All rights reserved. No reuse allowed without permission.

References

Adle-Biassette, H., Verney, C., Peoc'h, K., Dauge, M.-C., Razavi, F., Choudat, L., . . . Neurology, E. (2006). Immunohistochemical expression of prion protein (PrPC) in the human forebrain during development. *65*(7), 698-706.

Ambrosi, G., Cerri, S., & Blandini, F. J. J. o. n. t. (2014). A further update on the role of excitotoxicity in the pathogenesis of Parkinson's disease. *121*(8), 849-859.

Asante, E. A., Gowland, I., Grimshaw, A., Linehan, J. M., Smidak, M., Houghton, R., . . . Brandner, S. J. T. J. o. g. v. (2009). Absence of spontaneous disease and comparative prion susceptibility of transgenic mice expressing mutant human prion proteins. *90*(Pt 3), 546.

Chapman, J., Ben-Israel, J., Goldhammer, Y., & Korczyn, A. D. (1994). The risk of developing Creutzfeldt-Jakob disease in subjects with the PRNP gene codon 200 point mutation. *Neurology, 44*(9), 1683-1683.

Chiesa, R., Piccardo, P., Ghetti, B., & Harris, D. A. (1998). Neurological illness in transgenic mice expressing a prion protein with an insertional mutation. *Neuron, 21*(6), 1339-1351.

Cohen, F. E., & Prusiner, S. B. (1998). Pathologic conformations of prion proteins. *Annual Review of Biochemistry, 67*, 793-819.

Daude, N., Lehmann, S., & Harris, D. A. (1997). Identification of intermediate steps in the conversion of a mutant prion protein to a scrapie-like form in cultured cells. *Journal of Biological Chemistry, 272*, 11604-11612.

Fang, C., Wu, B., Le, N. T., Imberdis, T., Mercer, R. C., & Harris, D. A. J. P. p. (2018). Prions activate a p38 MAPK synaptotoxic signaling pathway. *14*(9), e1007283.

Foliaki, S. T., Groveman, B. R., Yuan, J., Walters, R., Zhang, S., Tesar, P., . . . Haigh, C. L. J. P. (2020). Pathogenic Prion Protein Isoforms Are Not Present in Cerebral Organoids Generated from Asymptomatic Donors Carrying the E200K Mutation Associated with Familial Prion Disease. *9*(6), 482.

Friedman-Levi, Y., Meiner, Z., Canello, T., Frid, K., Kovacs, G. G., Budka, H., . . . Gabizon, R. J. P. P. (2011). Fatal prion disease in a mouse model of genetic E200K Creutzfeldt-Jakob disease. *7*(11), e1002350.

Friedman-Levi, Y., Mizrahi, M., Frid, K., Binyamin, O., & Gabizon, R. (2013). PrPST, a soluble, protease resistant and truncated PrP form features in the pathogenesis of a genetic prion disease. *PLoS One, 8*(7), e69583.

bioRxiv preprint doi: https://doi.org/10.1101/2022.05.20.491674; this version posted May 23, 2022. The copyright holder for this preprint (which was not certified by peer review) is the author/funder. All rights reserved. No reuse allowed without permission.

Ghetti, B., Dlouhy, S. R., Giaccone, G., Bugiani, O., Frangione, B., Farlow, M. R., & Tagliavini, F. (1995). Gerstmann-Sträussler-Scheinker disease and the Indiana kindred. *Brain Pathology, 5*(1), 61-75.

Goldfarb, L. G., Petersen, R. B., Tabaton, M., Brown, P., LeBlanc, A. C., Montagna, P., . . . Gambetti, P. (1992). Fatal familial insomnia and familial Creutzfeldt-Jakob disease: disease phenotype determined by a DNA polymorphism. *Science, 258*, 806-808.

Gonzalez, C., Armijo, E., Bravo-Alegria, J., Becerra-Calixto, A., Mays, C. E., & Soto, C. (2018). Modeling amyloid beta and tau pathology in human cerebral organoids. *Molecular Psychiatry, 23*(12), 2363-2374.

Goold, R., Rabbanian, S., Sutton, L., Andre, R., Arora, P., Moonga, J., . . . Collinge, J. J. N. c. (2011). Rapid cell-surface prion protein conversion revealed using a novel cell system. *2*(1), 1-11.

Groveman, B. R., Foliaki, S. T., Orru, C. D., Zanusso, G., Carroll, J. A., Race, B., & Haigh, C. L. J. A. n. c. (2019). Sporadic Creutzfeldt-Jakob disease prion infection of human cerebral organoids. *7*(1), 1-12.

Hynd, M. R., Scott, H. L., & Dodd, P. R. J. N. i. (2004). Glutamate-mediated excitotoxicity and neurodegeneration in Alzheimer's disease. *45*(5), 583-595.

Jones, E., Hummerich, H., Viré, E., Uphill, J., Dimitriadis, A., Speedy, H., . . . Whitfield, J. (2020). Identification of novel risk loci and causal insights for sporadic Creutzfeldt-Jakob disease: a genome-wide association study. *The Lancet Neurology, 19*(10), 840-848.

Kamali-Jamil, R., Vázquez-Fernández, E., Tancowny, B., Rathod, V., Amidian, S., Wang, X., . . . Hornemann, S. J. P. p. (2021). The ultrastructure of infectious L-type bovine spongiform encephalopathy prions constrains molecular models. *17*(6), e1009628.

Khosravani, H., Zhang, Y., Tsutsui, S., Hameed, S., Altier, C., Hamid, J., . . . Zamponi, G. W. (2008). Prion protein attenuates excitotoxicity by inhibiting NMDA receptors. *Journal of Cell Biology, 181*(3), 551-565.

Kim, M.-O., Takada, L. T., Wong, K., Forner, S. A., & Geschwind, M. D. J. C. S. H. p. i. b. (2018). Genetic PrP prion diseases. *10*(5), a033134.

King, A. E., Woodhouse, A., Kirkcaldie, M. T., & Vickers, J. C. J. E. n. (2016). Excitotoxicity in ALS: overstimulation, or overreaction? *, 275*, 162-171.

Kornau, H.-C., Schenker, L. T., Kennedy, M. B., & Seeburg, P. H. J. S. (1995). Domain interaction between NMDA receptor subunits and the postsynaptic density protein PSD-95. *269*(5231), 1737-1740.

bioRxiv preprint doi: https://doi.org/10.1101/2022.05.20.491674; this version posted May 23, 2022. The copyright holder for this preprint (which was not certified by peer review) is the author/funder. All rights reserved. No reuse allowed without permission.

Kovacs, G. G., Rahimi, J., Ströbel, T., Lutz, M. I., Regelsberger, G., Streichenberger, N., . . . Budka, H. J. B. P. (2017). Tau pathology in Creutzfeldt-Jakob disease revisited. *27*(3), 332-344.

Kovacs, G. G., Seguin, J., Quadrio, I., Höftberger, R., Kapás, I., Streichenberger, N., . . . Vandenberghe, R. J. A. n. (2011). Genetic Creutzfeldt-Jakob disease associated with the E200K mutation: characterization of a complex proteinopathy. *121*(1), 39-57.

Kraus, A., Hoyt, F., Schwartz, C. L., Hansen, B., Artikis, E., Hughson, A. G., . . . Caughey, B. J. M. C. (2021). High-resolution structure and strain comparison of infectious mammalian prions.

Lau, A., McDonald, A., Daude, N., Mays, C. E., Walter, E. D., Aglietti, R., . . . Yang, J. (2015). Octarepeat region flexibility impacts prion function, endoproteolysis and disease manifestation. *EMBO molecular medicine, 7*(3), 339-356.

Lehmann, S., & Harris, D. A. (1996a). Mutant and infectious prion proteins display common biochemical properties in cultured cells. *Journal of Biological Chemistry, 271*, 1633-1637.

Lehmann, S., & Harris, D. A. (1996b). Two mutant prion proteins expressed in cultured cells acquire biochemical properties reminiscent of the scrapie isoform. *Proc. Natl. Acad. Sci. USA, 93*, 5610-5614.

Li, B., Otsu, Y., Murphy, T. H., & Raymond, L. A. J. J. o. N. (2003). Developmental decrease in NMDA receptor desensitization associated with shift to synapse and interaction with postsynaptic density-95. *23*(35), 11244-11254.

Matamoros-Angles, A., Gayosso, L. M., Richaud-Patin, Y., di Domenico, A., Vergara, C., Hervera, A., . . . Gavín, R. (2018). iPS Cell cultures from a Gerstmann-Sträussler-Scheinker patient with the Y218N PRNP mutation recapitulate tau pathology. *Molecular Neurobiology, 55*(4), 3033-3048.

Mead, S., Lloyd, S., & Collinge, J. (2019). Genetic factors in mammalian prion diseases. *Annual review of genetics, 53*, 117-147.

Meisl, G., Kurt, T., Condado-Morales, I., Bett, C., Sorce, S., Nuvolone, M., . . . Cohen, S. I. (2021). Scaling analysis reveals the mechanism and rates of prion replication in vivo. *Nature Structural & Molecular Biology, 28*(4), 365-372.

Mercer, R. C., McDonald, A. J., Bove-Fenderson, E., Fang, C., Wu, B., & Harris, D. A. (2018a). Prion diseases. In *The Molecular and Cellular Basis of Neurodegenerative Diseases* (pp. 23-56): Elsevier.

Mercer, R. C., Daude, N., Dorosh, L., Fu, Z.-L., Mays, C. E., Gapeshina, H., . . . Cashman, N. R. J. P. p. (2018b). A novel Gerstmann-Sträussler-Scheinker disease mutation defines a precursor for amyloidogenic 8 kDa PrP fragments and reveals N-terminal structural changes shared by other GSS alleles. *14*(1), e1006826.

bioRxiv preprint doi: https://doi.org/10.1101/2022.05.20.491674; this version posted May 23, 2022. The copyright holder for this preprint (which was not certified by peer review) is the author/funder. All rights reserved. No reuse allowed without permission.

Mercer, R. C., & Harris, D. A. (2019). Identification of anti-prion drugs and targets using toxicity-based assays. *Current opinion in pharmacology, 44*, 20-27.

Minikel, E. V., Vallabh, S. M., Lek, M., Estrada, K., Samocha, K. E., Sathirapongsasuti, J. F., . . . Gambetti, P. J. S. t. m. (2016). Quantifying prion disease penetrance using large population control cohorts. *8*(322), 322ra329-322ra329.

Orrú, C. D., Groveman, B. R., Raymond, L. D., Hughson, A. G., Nonno, R., Zou, W., . . . Caughey, B. J. P. P. (2015). Bank vole prion protein as an apparently universal substrate for RT-QuIC-based detection and discrimination of prion strains. *11*(6), e1004983.

Palmer, M. S., Dryden, A. J., Hughes, J. T., & Collinge, J. (1991). Homozygous prion protien genotype predisposes to sporadic Cretuzfeldt-Jakob disease. *Nature, 352*, 340-342.

Park, S., & Mostoslavsky, G. J. C. p. i. s. c. b. (2018). Generation of Human Induced Pluripotent Stem Cells Using a Defined, Feeder-Free Reprogramming System. *45*(1), e48.

Prusiner, S. B. (1998). Prions. *Proc. Natl. Acad. Sci. USA, 95*, 13363-13383.

Rosenmann, H., Talmor, G., Halimi, M., Yanai, A., Gabizon, R., & Meiner, Z. (2001). Prion protein with an E200K mutation displays properties similar to those of the cellular isoform PrP^{C}. *Journal of Neurochemistry, 76*(6), 1654-1662.

Schätzl, H. M., Laszlo, L., Holtzman, D. M., Tatzelt, J., DeArmond, S. J., Weiner, R. I., . . . Prusiner, S. B. (1997). A hypothalamic neuronal cell line persistently infected with scrapie prions exhibits apoptosis. *Journal of Virology, 71*(11), 8821-8831.

Sepers, M. D., & Raymond, L. A. J. D. d. t. (2014). Mechanisms of synaptic dysfunction and excitotoxicity in Huntington's disease. *19*(7), 990-996.

Shi, Y., Kirwan, P., & Livesey, F. J. J. N. p. (2012). Directed differentiation of human pluripotent stem cells to cerebral cortex neurons and neural networks. *7*(10), 1836-1846.

Somers, A., Jean, J. C., Sommer, C. A., Omari, A., Ford, C. C., Mills, J. A., . . . Smith, B. W. J. S. c. (2010). Generation of transgene-free lung disease-specific human induced pluripotent stem cells using a single excisable lentiviral stem cell cassette. *28*(10), 1728-1740.

Sommer, A. G., Rozelle, S. S., Sullivan, S., Mills, J. A., Park, S.-M., Smith, B. W., . . . Gadue, P. J. J. (2012). Generation of human induced pluripotent stem cells from peripheral blood using the STEMCCA lentiviral vector. (68), e4327.

Sommer, C. A., Christodoulou, C., Gianotti-Sommer, A., Shen, S. S., Sailaja, B. S., Hezroni, H., . . . Mostoslavsky, G. J. P. O. (2012). Residual expression of reprogramming factors affects the transcriptional program and epigenetic signatures of induced pluripotent stem cells. *7*(12), e51711.

bioRxiv preprint doi: https://doi.org/10.1101/2022.05.20.491674; this version posted May 23, 2022. The copyright holder for this preprint (which was not certified by peer review) is the author/funder. All rights reserved. No reuse allowed without permission.

Sommer, C. A., Stadtfeld, M., Murphy, G. J., Hochedlinger, K., Kotton, D. N., & Mostoslavsky, G. J. S. c. (2009). Induced pluripotent stem cell generation using a single lentiviral stem cell cassette. *27*(3), 543-549.

Staerk, J., Dawlaty, M. M., Gao, Q., Maetzel, D., Hanna, J., Sommer, C. A., . . . Jaenisch, R. J. C. s. c. (2010). Reprogramming of peripheral blood cells to induced pluripotent stem cells. *7*(1), 20.

Steele, A. D., Emsley, J. G., Ozdinler, P. H., Lindquist, S., & Macklis, J. D. (2006). Prion protein (PrP^C) positively regulates neural precursor proliferation during developmental and adult mammalian neurogenesis. *Proc. Natl. Acad. Sci. USA, 103*(9), 3416-3421.

Takahashi, K., Tanabe, K., Ohnuki, M., Narita, M., Ichisaka, T., Tomoda, K., & Yamanaka, S. J. c. (2007). Induction of pluripotent stem cells from adult human fibroblasts by defined factors. *131*(5), 861-872.

Taraboulos, A., Jendroska, K., Serban, D., Yang, S.-L., DeArmond, S. J., & Prusiner, S. B. (1992). Regional mapping of prion proteins in brain. *Proc. Natl. Acad. Sci. USA, 89*, 7620-7624.

Thomson, J. A., Itskovitz-Eldor, J., Shapiro, S. S., Waknitz, M. A., Swiergiel, J. J., Marshall, V. S., & Jones, J. M. J. s. (1998). Embryonic stem cell lines derived from human blastocysts. *282*(5391), 1145-1147.

Tremblay, P., Bouzamondo-Bernstein, E., Heinrich, C., Prusiner, S. B., & DeArmond, S. J. J. B. r. (2007). Developmental expression of PrP in the post-implantation embryo. *1139*, 60-67.

Vázquez-Fernández, E., Vos, M. R., Afanasyev, P., Cebey, L., Sevillano, A. M., Vidal, E., . . . Peters, P. J. J. P. p. (2016). The structural architecture of an infectious mammalian prion using electron cryomicroscopy. *12*(9), e1005835.

Veith, N. M., Plattner, H., Stuermer, C. A., Schulz-Schaeffer, W. J., & Bürkle, A. J. E. j. o. c. b. (2009). Immunolocalisation of PrPSc in scrapie-infected N2a mouse neuroblastoma cells by light and electron microscopy. *88*(1), 45-63.

Wadsworth, J. D., & Collinge, J. (2007). Update on human prion disease. *Biochimica et Biophysica Acta (BBA)-Molecular Basis of Disease, 1772*(6), 598-609.

Watts, J. C., & Prusiner, S. B. (2017). Experimental models of inherited PrP prion diseases. *Cold Spring Harbor perspectives in medicine, 7*(11), a027151.

Yamanaka, S. J. C. s. c. (2012). Induced pluripotent stem cells: past, present, and future. *10*(6), 678-684.

Yang, W., Cook, J., Rassbach, B., Lemus, A., DeArmond, S. J., & Mastrianni, J. A. (2009). A new transgenic mouse model of Gerstmann-Straussler-Scheinker syndrome caused by the A117V mutation of PRNP. *Journal of Neuroscience, 29*(32), 10072-10080.

bioRxiv preprint doi: https://doi.org/10.1101/2022.05.20.491674; this version posted May 23, 2022. The copyright holder for this preprint (which was not certified by peer review) is the author/funder. All rights reserved. No reuse allowed without permission.

Figure Legends

Figure 1: Generation of an iPSC library from a kindred harbouring the E200K mutation of PrP

(A) Schematic representation of the reprograming of peripheral blood mononuclear cells (PBMC) to induced pluripotent stem cells (iPSC). Sev, Sendai virus. **(B)** Representative immunofluorescence staining of TRA-1-81 from five non-carrier iPSC lines (NC10, NC11, NC12, BU1, BU3) and seven iPSC lines carrying the E200K mutation (CJD2, CJD3, CJD4, CJD5, CJD6, CJD29, CJD40) that were used in this study. Scale bars = 100 µm.

Figure 2: Differentiation of human iPSCs to pyramidal cortical neurons

(A) Schematic representation of iPSC differentiation into neuronal progenitors and neurons. **(B)** Example of electrophysiological properties of neurons at different stages of terminal differentiation. Typical single-cell, patch-clamp recordings from neurons at a range of ages following neuronal differentiation. Young neurons (day 75), fire a single action potential following current injection. As neurons mature, they progress from firing a short burst of action potentials in response to current injection (day 97) to sustained action potential firing (day 110). **(C i-v)** Morphological change in iPSCs cultures during neuronal induction. **(i)** Confluent monolayer of iPSCs ready for neural induction, **(ii)** iPSC-derived progenitor cells after neuronal induction, **(iii)** neurogenesis stage, **(iv)** neurons at day 95, **(v)** immunofluorescence staining for F-actin visualizes dendritic spine morphology of mature neurons at day 105. Each boxed region in panels **v** and **v1** is shown at higher magnification in the smaller panels to the bottom and right respectively. **(vi, ix)** Immunofluorescence staining for different progenitor makers. **(vi)** Pax6^{+}/ Nestin^{+} primary

bioRxiv preprint doi: https://doi.org/10.1101/2022.05.20.491674; this version posted May 23, 2022. The copyright holder for this preprint (which was not certified by peer review) is the author/funder. All rights reserved. No reuse allowed without permission.

progenitor cells forming a rosette structure at day 29, **(ix)** TBR2$^+$/Nestin$^+$ secondary progenitor cells at day 40. **(vii, viii, x, xi)** Immunofluorescence staining for different classes of excitatory neurons. The glutamatergic identity of young **(vii, x)** and mature neurons **(viii, xi)** was confirmed by immunofluorescent staining for the vesicular glutamate transporter 1 (Vglut1), neuron specific tubulin (Tuj1), dendritic marker (Map2) and cortical upper-layer neuron marker (Satb2). Nuclei in **v-xi** are stained with DAPI. These images were acquired from a differentiation of line BU1.

Figure 3: Biochemical properties of PrP expressed by iPSC derived cortical neurons

(A) Expression level of PrP is similar among lines of IPSCs-derived neurons. Western blotting analysis for total PrP levels in lysates from neurons at 95 days post differentiation. The anti-PrP antibody D18 was used. **(B)** Exposure of neuronal lysates to proteinase K. 50 µg of total protein was exposed to 2.5 µg/ml PK for 1 hour at 37 ℃ with orbital shaking at 750 rpm. The blot was probed with the anti-PrP antibody D18. **(C)** Detergent extracts were centrifuged at 186 000 x g for 1 hour at 4 ℃. Soluble and insoluble fractions were collected and analyzed by western blot. The blot was probed with the anti-PrP antibody D18.

Figure 4: iPSC-derived neurons from E200K carriers accumulate abnormal forms of PrP

Representative images of immunofluorescent staining of PrP (D18 antibody; red) and ThS (yellow). **(A)** Uninfected N2a and ScN2a cells with and without exposure to PK. Arrows

bioRxiv preprint doi: https://doi.org/10.1101/2022.05.20.491674; this version posted May 23, 2022. The copyright holder for this preprint (which was not certified by peer review) is the author/funder. All rights reserved. No reuse allowed without permission.

indicate accumulations of misfolded PrP. **(B)** iPSC derived neurons from individuals carrying the E200K mutation following exposure to PK. **(C)** iPSC derived neurons from non-carriers stained following exposure to PK. **(D)** Quantification of the number of PrP and ThS positive puncta following exposure to PK from B and C. Non-carriers unrelated to the kindred are indicated in green, non-carriers in the kindred in blue and E200K carriers in red. p=0.0017 (BU + NC vs. E200K) and 0.02 (NC vs. E200K). n=fields observed. BU1 n=9; BU3 n=6, NC10 n=4; NC11 n=4; NC12 n=4; CJD2 n=4; CJD3 n=14; CJD4 n=3; CJD5 n=3; CJD6 n=9; CJD29 n=14; CJD40 n=12. Mean +/- SEM is plotted. Scale bars = 10 µm

Figure 5: Seeding activity of cell lysates of human iPSC derived neurons

Seeding activity is assessed using the Real Time-Quaking Induced Conversion (RT-QuIC) assay. **(A)** Sensitivity of the assay is demonstrated by a positive result using a 10^{-7} dilution of brain homogenate from a mouse at end-stage RML prion infection. n = 5 wells per sample. A 10^{-4} dilution of uninfected, normal brain homogenate (NBH) is used as a negative control. **(B)** RT-QuIC is capable of detecting seeding activity in as little as 2 pg of total protein from lysates of chronically RML infected N2a cells (ScN2a). Uninfected N2a cell lysate is used as a negative control. n = 5 wells per sample. **(C)** No seeding activity was detected in lysates of 95 day post differentiation iPSC derived cortical neurons. n = 5 wells seeded with 2 ng protein per sample. All experiments were performed using full length (23-231) recombinant bank vole PrP. Mean thioflavin T fluorescence as a percentage of maximum signal is plotted against time in hours.

bioRxiv preprint doi: https://doi.org/10.1101/2022.05.20.491674; this version posted May 23, 2022. The copyright holder for this preprint (which was not certified by peer review) is the author/funder. All rights reserved. No reuse allowed without permission.

Figure 6: E200K PrP expressing neurons show misaligned postsynaptic markers. Representative immunofluorescent images following staining of iPSC derived cortical neurons for NMDAR1 and PSD95. NMDAR1 staining is shown in green, PSD95 staining is shown in red. **(A)** E200K carriers **(B)** non-carriers. Scale bars = 5 µm. **(C)** Graph of pixel intensities for each fluorescent channel along a representative segment of dendrite from an E200K carrier (lower panel) and a non-carrier (upper panel). Areas with significant overlap of fluorescent signal, indicated by boxes, are scored as co-localized. Black arrows indicate regions of low colocalization. **(D)** Plot showing a significant reduction in the colocalization of NMDAR1 and PSD95 along the dendritic shaft of neurons expressing E200K PrP. p=0.007 (BU + NC vs. E200K) and p=0.04 (NC vs. E200K). n=fields observed. BU1 n=13; BU3 n=6, NC10 n=10; NC11 n=9; NC12 n=9; CJD2 n=9; CJD3 n=22; CJD5 n=9; CJD6 n=9; CJD29 n=30; CJD40 n=14. **(E)** Plot of the number of postsynaptic NMDAR1 Clusters per 10 µm. Non-carriers unrelated to the kindred are indicated in green, kindred non-carriers are in blue and E200K carriers are in red. p=0.26 (BU + NC vs. E200K) and p=0.18 (NC vs. E200K). n=fields observed. BU1 n=13; BU3 n=6, NC10 n=10; NC11 n=9; NC12 n=9; CJD2 n=9; CJD3 n=22; CJD5 n=9; CJD6 n=9; CJD29 n=30; CJD40 n=14. **(F)** Plot of the number of postsynaptic PSD95 clusters per 10 µm. p=0.56 (BU + NC vs. E200K) and p=0.75 (NC vs. E200K). n=fields observed. BU1 n=8; BU3 n=6, NC10 n=17; NC11 n=14; NC12 n=11; CJD2 n=11; CJD3 n=23; CJD5 n=10; CJD6 n=19; CJD29 n=16; CJD40 n=12. Mean +/- SEM is plotted for all graphs.

bioRxiv preprint doi: https://doi.org/10.1101/2022.05.20.491674; this version posted May 23, 2022. The copyright holder for this preprint (which was not certified by peer review) is the author/funder. All rights reserved. No reuse allowed without permission.

Table 1: Individuals represented in the iPSC library

Sample ID	Presentation[a]	*PRNP* codon 129	Mutation	Used in Study?
NC10	none	MV	none	yes
NC11	none	MM	none	yes
NC12	none	MV	none	yes
NC14	none	MV	none	no
NC16	none	MV	none	no
NC17	none	MV	none	no
NC18	none	MV	none	no
NC22	none	VV	none	no
NC25	none	MV	none	no
NC32	none	MV	none	no
NC33	none	MV	none	no
CJD2	asymptomatic	MV	E200K	yes
CJD3	asymptomatic	MM	E200K	yes
CJD4	asymptomatic	MV	E200K	yes
CJD5	asymptomatic	MV	E200K	yes
CJD6	asymptomatic	MV	E200K	yes
CJD9	asymptomatic	MV	E200K	no
CJD13	asymptomatic	MM	E200K	no
CJD20	asymptomatic	MV	E200K	no
CJD24	asymptomatic	MM	E200K	no
CJD29	asymptomatic	MM	E200K	yes
CJD40	asymptomatic	MM	E200K	yes
BU1	N/A	MV	none	Yes
BU3	N/A	MM	none	Yes

[a]Clinical presentation at time of collection

was not certified by peer review) is the author/funder. All rights reserved. No reuse allowed without permission.

Figure 1: Generation of a CJD-E200K iPSC library from a kindred harbouring the E200K mutation of PrP

A

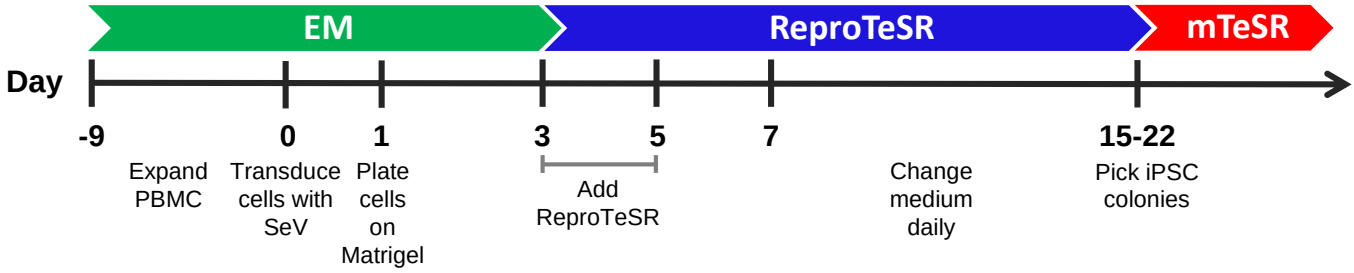

B

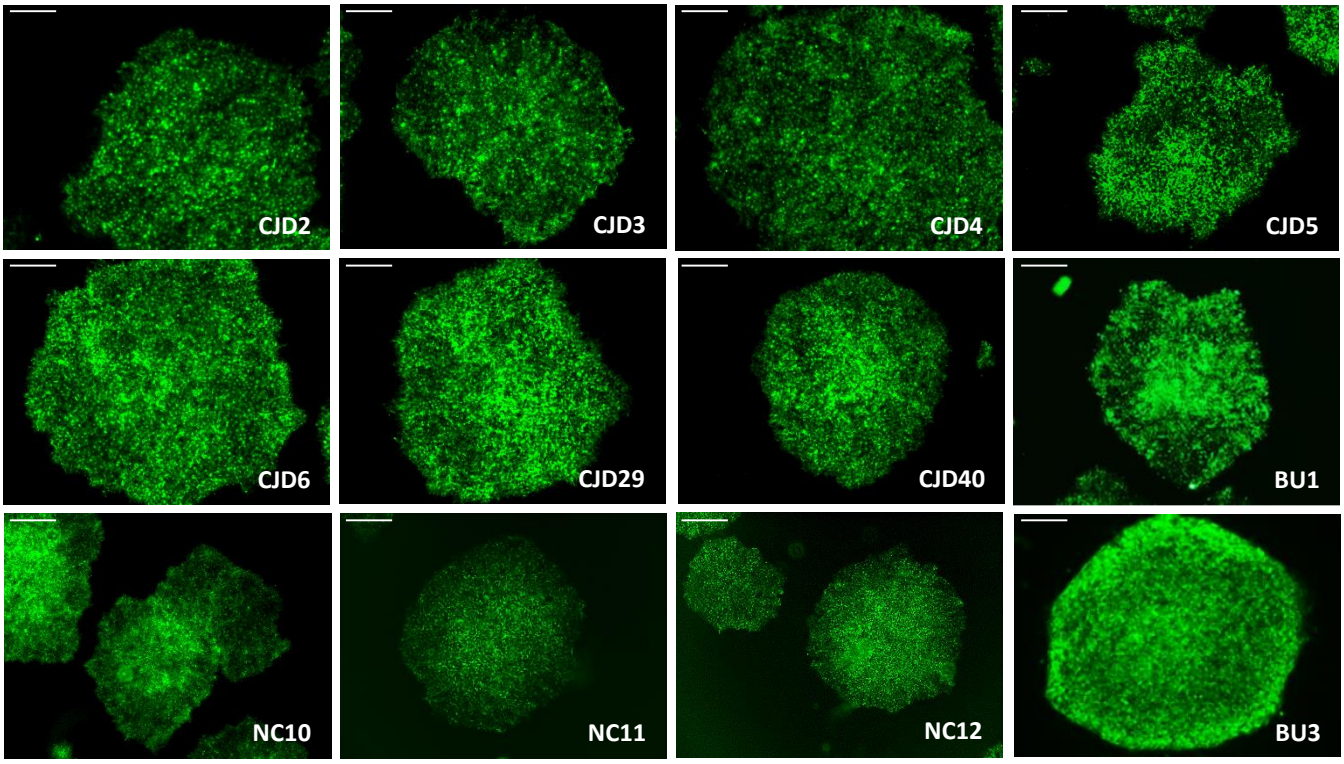

was not certified by peer review) is the author/funder. All rights reserved. No reuse allowed without permission.

Figure 2: Differentiation of human iPSCs to pyramidal cortical neurons

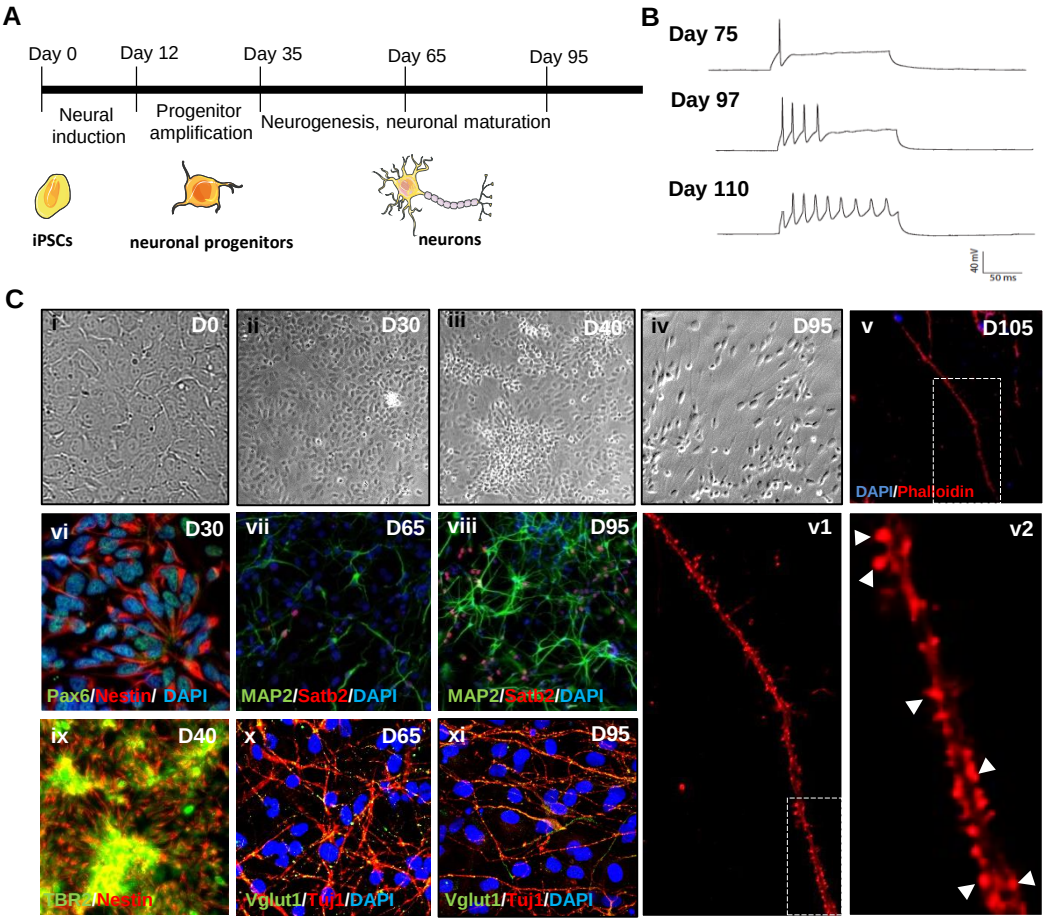

was not certified by peer review) is the author/funder. All rights reserved. No reuse allowed without permission.

Figure 3: Biochemical properties of PrP expressed by iPSC derived cortical neurons

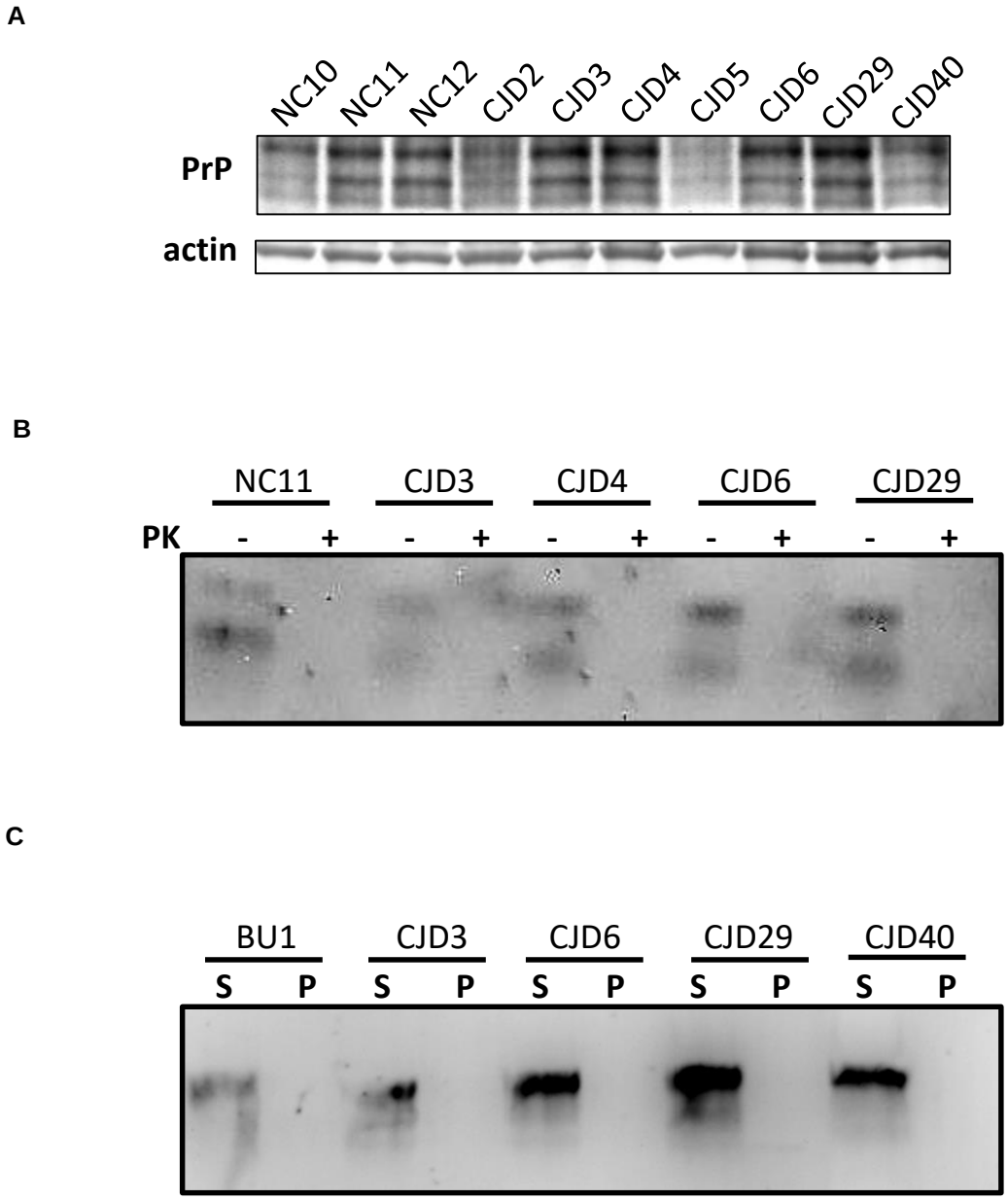

was not certified by peer review) is the author/funder. All rights reserved. No reuse allowed without permission.

Figure 4: iPSC-derived neurons from E200K carriers accumulate abnormal forms of PrP

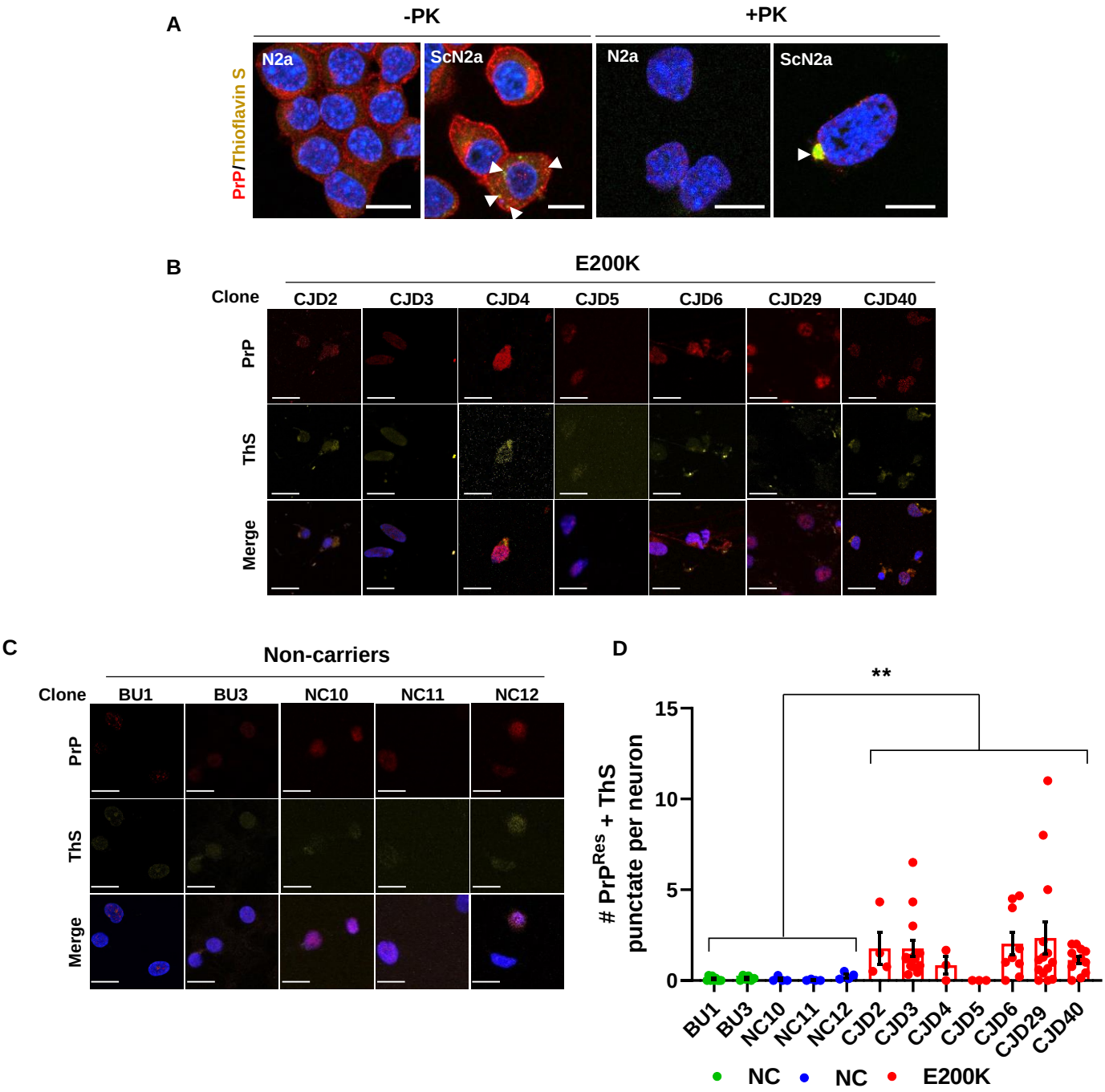

was not certified by peer review) is the author/funder. All rights reserved. No reuse allowed without permission.

Figure 5: Seeding activity of cell lysates of human iPSC derived neurons

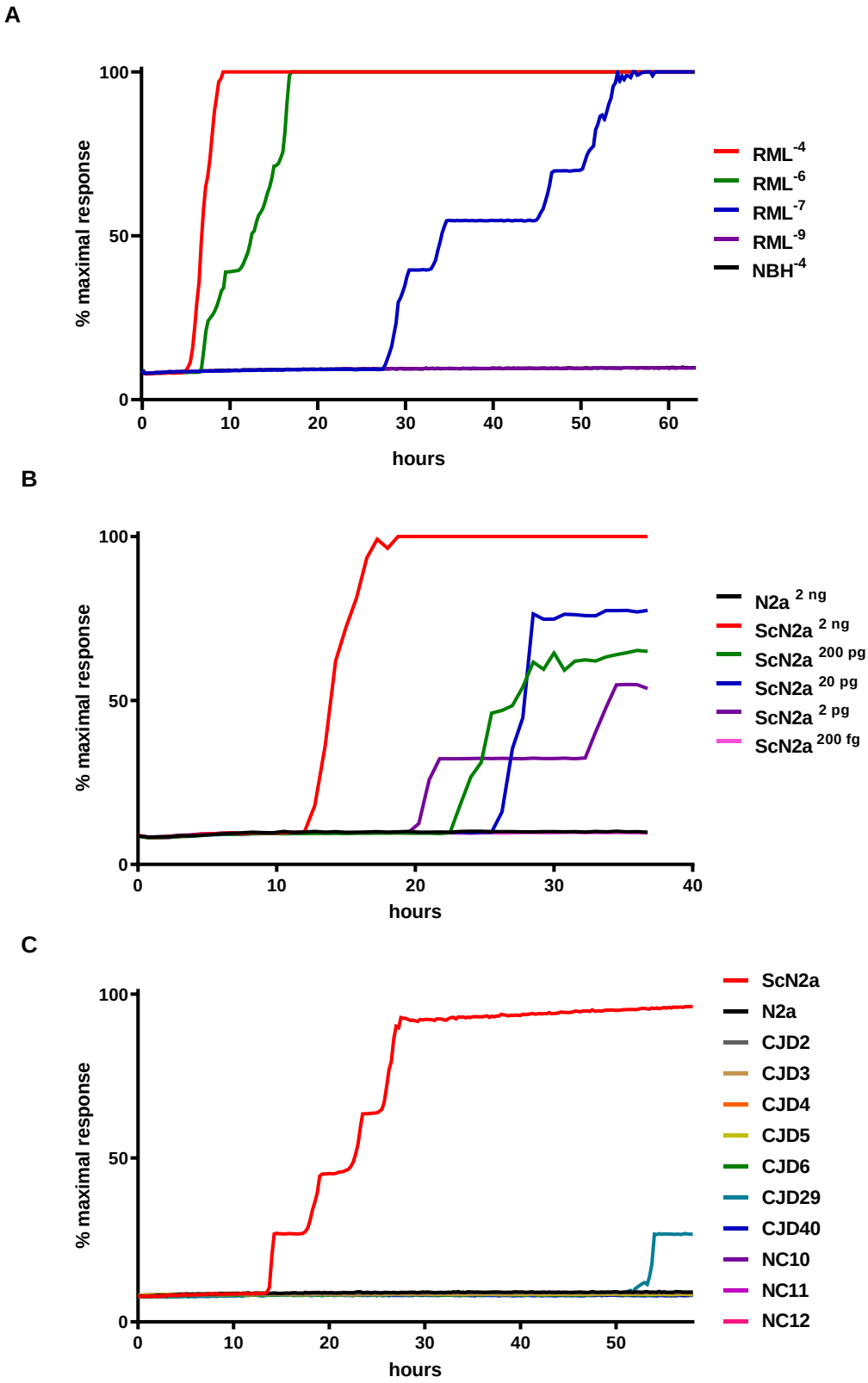

was not certified by peer review) is the author/funder. All rights reserved. No reuse allowed without permission.
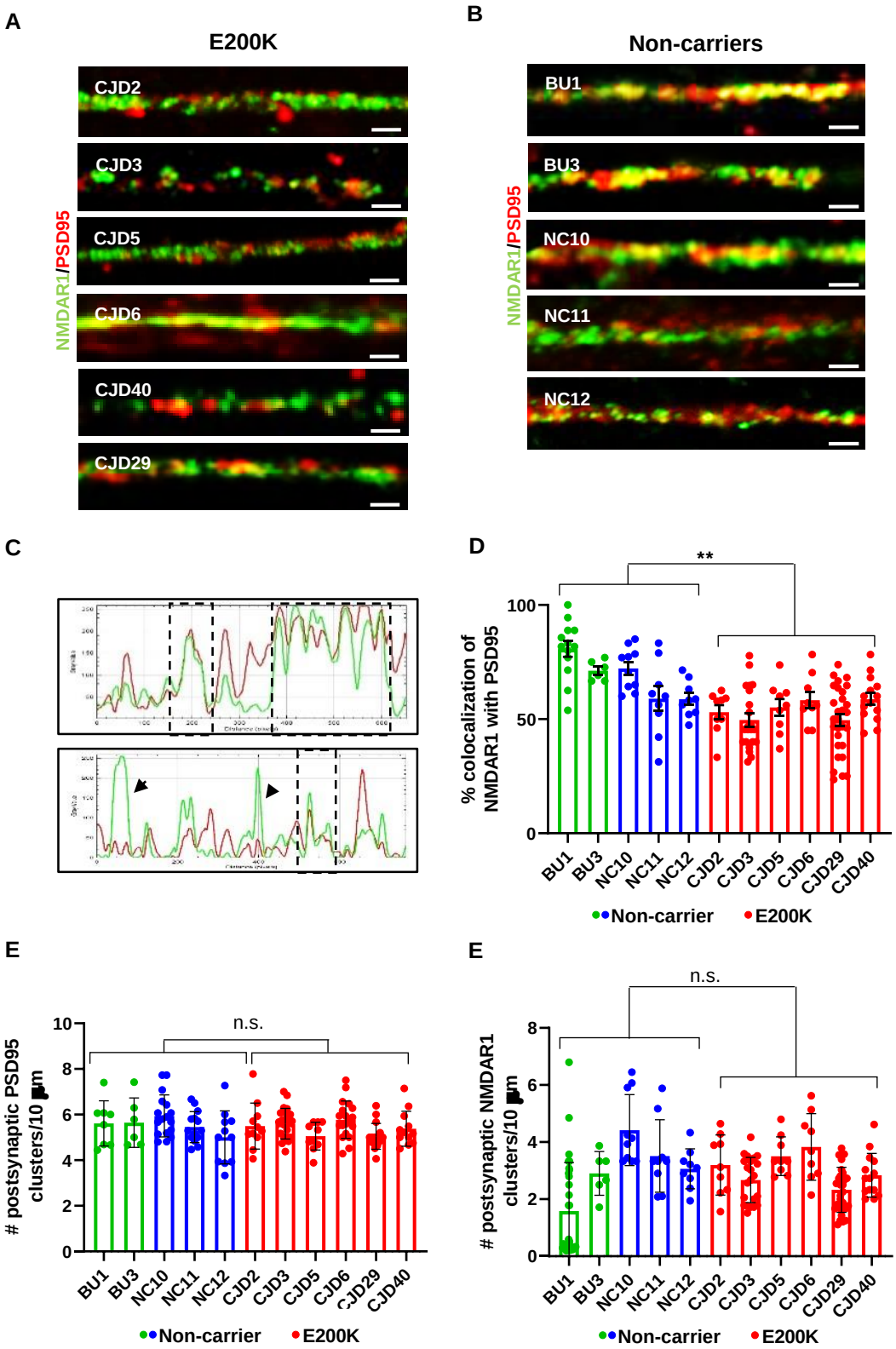
Figure 6: E200K PrP expressing neurons have a destabilized postsynaptic site